Zhu *et al. Satellite Navigation* (2022) 3:27
https://doi.org/10.1186/s43020-022-00088-w

Satellite Navigation
https://satellite-navigation.springeropen.com/

ORIGINAL ARTICLE

Open Access

Refining the ERA5-based global model for vertical adjustment of zenith tropospheric delay

Ge Zhu[1], Liangke Huang[1*], Yunzhen Yang[2], Junyu Li[1], Lv Zhou[1] and Lilong Liu[1*]

Abstract

Tropospheric delay is an important factor affecting high precision Global Navigation Satellite System (GNSS) positioning and also the basic data for GNSS atmospheric research. However, the existing tropospheric delay models have some problems, such as only a single function used for the entire atmosphere. In this paper, an ERA5-based (the fifth generation of European Centre for Medium-Range Weather Forecasts Reanalysis) global model for vertical adjustment of Zenith Tropospheric Delay (ZTD) using a piecewise function is developed. The ZTD data at 611 radiosonde stations and the MERRA-2 (second Modern-Era Retrospective analysis for Research and Applications) atmospheric reanalysis data were used to validate the model reliability. The Global Zenith Tropospheric Delay Piecewise (GZTD-P) model has excellent performance compared with the Global Pressure and Temperature (GPT3) model. Validated at radiosonde stations, the performance of the GZTD-P model was improved by 0.96 cm (23%) relative to the GPT3 model. Validated with MERRA-2 data, the quality of the GZTD-P model is improved by 1.8 cm (50%) compared to the GPT3 model, showing better accuracy and stability. The ZTD vertical adjustment model with different resolutions was established to enrich the model's applicability and speed up the process of tropospheric delay calculation. By providing model parameters with different resolutions, users can choose the appropriate model according to their applications.

Keywords: Piecewise function, Vertical adjustment, ZTD, GNSS, Tropospheric delay

Introduction

Tropospheric delay is an important factor affecting the high precision of space technologies and also the key aspect of atmospheric scientific research (Ding, 2020; Huang et al., 2012; Li et al., 2021; Nafisi et al., 2012; Xia et al., 2019; Zhang et al., 2020; Zhou et al., 2021). Depending on the elevation angle of a satellite, its effect ranges from two to twenty meters (Huang et al., 2021a; Zhao et al., 2014). Therefore, a high precision tropospheric delay model is beneficial for Global Navigation Satellite System (GNSS) positioning and atmospheric water vapor sensing (Huang et al., 2021b; Jin & Su, 2020; Mohammed et al., 2022; Tang et al., 2013; Yang et al., 2020; Zhang et al., 2018; Zhou et al., 2020; Zhu et al., 2021).

The existing tropospheric delay models can be classified into three categories. The first one is numerical weather modeling, for instance the Vienna Mapping Functions (VMF) (Böhm et al., 2006) and the Potsdam Mapping Factors (PMF) (Zus et al., 2014). The second one is analytical modeling with in-situ meteorological observations, like the Hopfield model (1969), the Saastamoinen model (1972), and the Black model (1978). The third category includes empirical models, such as the University of New Brunswick (UNB) series models (Leandro et al., 2006, 2008), European Geostationary Navigation Overlay Service (EGNOS) model (Penna et al., 2001), TropGrid series models (Krueger et al., 2004; Schüler et al., 2014), Global Pressure and Temperature (GPT) series models (Böhm et al., 2007, 2015; Lagler et al.,

*Correspondence: lkhuang666@163.com; hn_liulilong@163.com

[1] College of Geomatics and Geoinformation, Guilin University of Technology, Guilin 541004, China
Full list of author information is available at the end of the article

2013; Landskron et al., 2018), and Saastamoinen + GPT3 model. The UNB3 model stores meteorological parameters in tabular form and divides the world into five latitude bands. Krueger et al. (2004) developed the TropGrid model using National Centers for Environmental Prediction (NCEP) atmospheric reanalysis data, and the quality of the TropGrid model is superior to that of the EGNOS model. Schüler et al. (2014) added the diurnal variation of the tropospheric delay to the TropGrid model and constructed the TropGrid2 model. This model improves the temporal resolution of the model but ignores the semi-annual variation in tropospheric delay. GPT3 is the latest generation model of GPT series, which is an upgraded version of GPT2w, and has long been recognized as the high precision tropospheric delay model (Ding and Chen, 2020; Sun et al., 2019).

Song et al. (2011) built the Shanghai Astronomical Observatory (SHAO) model based on the European Centre for Medium-Range Weather Forecasts (ECMWF) atmospheric reanalysis data, whose accuracy was improved by 60.5% compared to the EGNOS model. Li et al. (2018) introduced a new method to simulate ZTD vertical characteristics and constructed a ZTD model of non-meteorological parameters named IGGtrop_SH. This new model improved the ZTD correction performance, especially in the Northern Hemisphere. Yao et al. (2016) recommended the Global Zenith Tropospheric Delay (GZTD2) model, considering the diurnal variation in the tropospheric delay. This model was validated using the International GNSS Service (IGS) data with its Root Mean Square (RMS) of 3.9 cm. Based on the Global Geodetic Observing System (GGOS) atmosphere data, Sun et al. (2017) developed the Global Zenith Tropospheric Delay Simplified (GZTDS) model with an assumption that the troposphere is a nonlinear system. The mean RMS of the GZTDS model, as validated with the IGS data, is 3.46 cm, equivalent to that of the GPT2w model.

In recent years, the data provided by atmospheric reanalysis products such as ERA-Interim, ERA5 (the fifth generation of European Centre for Medium-Range Weather Forecasts Reanalysis), NCEP, or MERRA-2 (the second Modern-Era Retrospective analysis for Research and Applications), have been widely used to obtain tropospheric delay information (Li et al., 2012, 2015; Yang et al., 2021; Zhou et al., 2020) as this method can obtain relatively accurate information. It is necessary to rely on the tropospheric delay model of high precision and high spatial and temporal resolution to obtain the tropospheric delay information at the location of a GNSS user by interpolating the information at the grid points to the GNSS sites (Li et al., 2016, 2017; Ma et al., 2021; Xia et al., 2020). Li and He, (2021) investigated the methods of deriving tropospheric parameters from the ERA-Interim surface data. Based on realistic assumptions on atmosphere structure, complicated formulas were proposed for vertical adjustment of pressure and PWV (Precipitable Water Vapor).

Since the tropospheric delay is dependent on the elevation, it varies at different atmospheric heights. However, the commonly used troposphere delay vertical profile model only uses a single function for the entire troposphere. Furthermore, it is difficult to reflect the change in tropospheric delay with respect to heights. Addressing these limitations in the previous models, this paper developed an ERA5-based global model for vertical adjustment of zenith tropospheric delay using a piecewise function.

Data

Radiosonde data

The radiosonde data provides the measured meteorological parameters at more than 1 500 stations around the world. The radiosonde data are obtained from the actual measurements of meteorological sensors on sounding balloons, which have high accuracy and reliability, and they are widely used to validate measurement results (Gui et al., 2017; Sun et al., 2019).

Atmospheric reanalysis product data

ERA5 includes atmospheric reanalysis data since 1979, which can be freely downloaded. Its pressure layer is divided into 37 sub-layers, which can provide key tropospheric parameters such as temperature, pressure, and specific humidity. Compared to the previous product ERA-Interim atmospheric reanalysis data, ERA5 can provide suitable surface parameters and vertical profile data, and its temporal resolution has increased from six-hour to one-hour.

MERRA-2 includes atmospheric reanalysis data since 1980, which can also be freely downloaded. Its pressure layer is divided into 42 sub-layers. (Randles et al., 2017; Molod et al., 2015).

Development of the GZTD-P model

For the better expression of the vertical profile of zenith tropospheric delay over the globe, negative exponential functions are often used to simulate the vertical change of the delay (Chen et al., 2020; Yao et al., 2013, 2016). To further verify the vertical change in the delays, two grid data points of the ERA5 atmospheric reanalysis data at 0:00 UTC (Universal Time Coordinated) on January 1, 2014, were randomly selected. The ZTD was obtained by the integration method on different pressure layers. An exponential function was used to fit the vertical change of the delays and the results are shown in Fig. 1. The exponential function, as well as the integration method

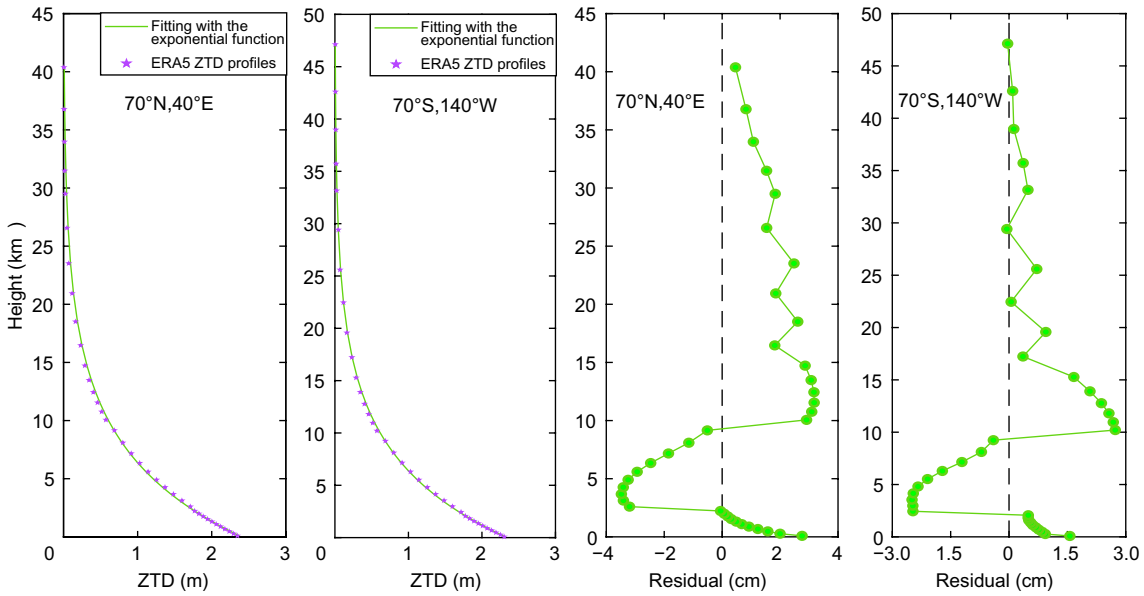

Fig. 1 ERA5 ZTD profiles and cures fitting with the exponential function at two grid points, and the corresponding fitting residual errors of the exponential function

(Thayer, 1974), are expressed as follows. The Saastamoinen model is introduced to obtain the ZHD (Zenith Hydrostatic Delay) above the top pressure level (Saastamoinen, 1972).

$$d^f_{\mathrm{ZTD}} = d^g_{\mathrm{ZTD}} \cdot \exp(a \cdot (H_f - H_g)) \tag{1}$$

$$e = S \cdot P/0.622 \tag{2}$$

$$N = k_1 \times (P - e)/T + k_2 \times e/T + k_3 \times e/T^2 \tag{3}$$

$$d_{\mathrm{ZTD}} = 1 \times 10^{-6} \int_{h_L}^{h_T} N \mathrm{d}H \tag{4}$$

$$d^T_{\mathrm{ZHD}} = \frac{2.2767 \times 10^{-3} \times P_T}{1 - 2.667 \times 10^{-3} \times \cos(2\varphi) - 2.8 \times 10^{-7} \times h_T} \tag{5}$$

where d^f_{ZTD} is the fitting result at height H_f (km), d^g_{ZTD} is the ZTD data at height H_g (km), and a is a parameter, N is the refractivity, P, e, S, T are the meteorological parameters, h_L is the lowest height, h_T is the topmost height, k_1, k_2, k_3 are the refractive index constants, d^T_{ZHD} is the ZHD above the top pressure level, and φ is the latitude.

Figure 1 shows that the vertical change of ZTD can be effectively simulated by a negative exponential function, but the ZTD at the two selected ERA5 grid points shows a poorer performance in the heights from 2 to 4 km. The largest fitting error reaches about –4 cm, and it also shows large fitting errors appear in the heights from about 9 km to 10 km, reaching about –3 cm. In order to simulate the vertical change in ZTD more accurately, a piecewise function is recommended to express the change in ZTD in different height intervals. Eight grid points are selected randomly to fit each elevation interval, and the optimal elevation interval is finally determined, which is divided into 0–3 km, 3–8 km, 8–16 km, and > 16 km. The piecewise function is expressed as follows:

$$d^t_{\mathrm{ZTD}} = \begin{cases} d^{r_1}_{\mathrm{ZTD}} \cdot \exp(H^s_1 \cdot (H_t - H_r)) & H_t < 3\ \mathrm{km} \\ d^{r_2}_{\mathrm{ZTD}} \cdot \exp(H^s_2 \cdot (H_t - H_r)) & 3\ \mathrm{km} \le H_t < 8\ \mathrm{km} \\ d^{r_3}_{\mathrm{ZTD}} \cdot \exp(H^s_3 \cdot (H_t - H_r)) & 8\ \mathrm{km} \le H_t < 16\ \mathrm{km} \\ d^{r_4}_{\mathrm{ZTD}} \cdot \exp(H^s_4 \cdot (H_t - H_r)) & H_t \ge 16\ \mathrm{km} \end{cases} \tag{6}$$

where H^s_1, H^s_2, H^s_3, H^s_4 represents the ZTD height scale factor, H_t represents the target height, H_r represents the reference height, d^t_{ZTD} represents the ZTD value at the target height, $d^{r_1}_{\mathrm{ZTD}}$, $d^{r_2}_{\mathrm{ZTD}}$, $d^{r_3}_{\mathrm{ZTD}}$, $d^{r_4}_{\mathrm{ZTD}}$ represents the ZTD values at the reference height in different elevation intervals, respectively.

The RMS of fitting error with the piecewise function and the exponential function at each elevation interval are shown in Table 1. As observed, the mean fitting error of the exponential function is about 20.7 mm, but the error can be effectively reduced by the piecewise function. It can be seen that the mean fitting error is the smallest in the 3–8 km elevation interval, only about 2.7 mm.

Table 1 The fitting error of piecewise function and exponential function

Coordinate	RMS of piecewise function and exponential function (mm)				
	0–3 km	3–8 km	8–16 km	> 16 km	Exponential function
70°N,40°E	7.2	2.8	8.4	3.2	22.6
70°N,80°E	8.7	2.9	9.8	3.0	21.8
40°N,140°W	9.8	0.5	8.4	3.2	16.9
40°N,100°W	9.8	1.0	7.9	2.9	25.1
40°S,40°E	12.5	1.9	8.1	3.1	19.3
40°S,80°E	9.8	2.3	7.4	3.1	24.0
70°S,140°W	8.2	2.0	9.8	3.0	15.5
70°S,100°W	10.6	3.2	9.7	3.0	22.5
Mean over the globe	10.4	2.7	9.0	3.1	20.7

The fitting errors of the exponential function and the piecewise function at the selected two grid points are displayed in Fig. 2.

Figure 2 exhibits that the piecewise function has a better fitting precision, and the performance is improved significantly in the lower heights compared to the exponential function. Therefore, the layered vertical profile information on ZTD calculated with the ERA5 atmospheric reanalysis data from 2012 to 2016 is used to develop the model. Some limitations remain in the current models, for instance the adoption of single gridded point data for modeling and the further optimization of model parameters. An approach based on the sliding window algorithm (Huang et al., 2019, 2021c) was applied to remove these limitations in the model.

In order to optimize the model parameters, a window size of $2^\circ \times 2^\circ$ is proposed, and the piecewise function is used for modeling in each height interval, considering the seasonal changes. The equation can be expressed as follows:

$$H_s = a_1 + a_2 \cdot \cos\left(2\pi \frac{t_{\mathrm{doy}}}{365.25}\right) + a_3 \cdot \sin\left(2\pi \frac{t_{\mathrm{doy}}}{365.25}\right) + a_4 \cdot \cos\left(4\pi \frac{t_{\mathrm{doy}}}{365.25}\right) + a_5 \cdot \sin\left(4\pi \frac{t_{\mathrm{doy}}}{365.25}\right) \tag{7}$$

In (7), H_s represents the ZTD height scale factor in each height interval, a_1, a_2, a_3, a_4, a_5 are the seasonal parameters, and t_{doy} is the day of year. The ERA5-based global model for vertical adjustment of zenith tropospheric delays using the piecewise function is developed, which is named GZTD-P model. The expression is shown in (6) and (7).

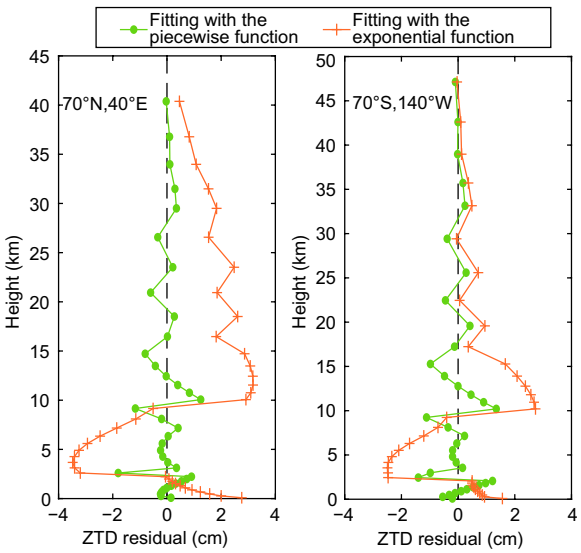

Fig. 2 The corresponding ZTD fit residual errors of the exponential function and piecewise function

Results and discussion

Accuracy verification of the GZTD-P model

Model validation at radiosonde stations

Taking the ZTD values of the layered profiles at 611 radiosonde stations around the world in 2017 and 2018 as reference values, the accuracy of the model in ZTD vertical adjustment at the radiosonde stations is validated. In the validation of the GZTD-P model and the GPT3 model, the ZTD are vertically interpolated from the surface layer to each layer at the radiosonde stations, continuing to the top layer of the radiosonde stations. The accuracies of the GZTD-P and the GPT3 models in the ZTD vertical interpolation of the radiosonde data in 2017 and 2018 are represented in Table 2 and Fig. 3.

As seen in Table 2, the GPT3 model has a negative average bias while the GZTD-P model has a positive average bias. The ZTD value obtained by the GPT3 model is smaller than the layered ZTD of the global radiosonde stations, and that obtained by the GZTD-P model is larger. The bias of the GZTD-P model was 0.64 cm, and the absolute value of the mean bias was reduced by 1.14 cm (64%) with the GPT3 model. The RMS of the GPT3 model is 4.16 cm, while the RMS of the GZTD-P model is 3.20 cm, which shows an increase in the accuracy by 0.96 cm (23%).

Figure 3 shows that the ZTD calculated with the GZTD-P model is larger than that at most radiosonde stations, and is smaller than that at the radiosonde stations over China. The GPT3 model has a clear negative bias in the Pacific Ocean, Antarctica, Oceania, southern

Table 2 The performance of the GZTD-P and GPT3 models validated at radiosonde stations

Models	Bias specifications (cm)			RMS specifications (cm)		
	Max	Min	Mean	Max	Min	Mean
GZTD-P	7.39	− 9.66	0.64	12.48	1.72	3.20
GPT3	5.27	− 13.35	− 1.78	15.76	1.53	4.16

Asia, and northern South America, indicating that the ZTD calculated with the GPT3 model in these areas is less than that at the radiosonde stations. Positive biases are seen in the Americas, central South America, and northern Asia, indicating that the ZTD values of the layered vertical interpolation calculated with the GPT3 model are greater than the ZTD values at the radiosonde stations in these areas. Both the GZTD-P model and the GPT3 model show obvious negative bias values in the China region, which could be attributed to the region's complex and changing climate and terrain. The GPT3 model exhibits small RMS values in North America, South America, Europe, Antarctica, and Oceania, but large RMS values in Asia, particularly China, which exhibits the greatest RMS error. Nonetheless, the GPT3 model continues to perform admirably around the world.

The GZTD-P model has small RMS values all over the world, particularly in North America, South America, Europe, and Oceania, indicating better accuracy. The GZTD-P model outperforms the GPT3 model in the Arctic Ocean, the western part of the Atlantic Ocean, the Pacific Ocean, and the northern part of Asia. The GPT3 model performs worse, which could be attributed to the complicated climate. The vertical change is also more complicated, and the GPT3 model struggles to detect the ZTD change accurately. Furthermore, because the piecewise function model can better simulate the vertical variation characteristics of tropospheric delays in different height intervals, a certain improvement of GZTD-P model is shown for the areas of China with large terrain fluctuations.

Because the zenith tropospheric delay is much related to heights, we divided the troposphere into nine height intervals to further analyze the accuracy changes of models at different heights. Elevations greater than 32 km are separately combined into one height interval. Figure 4 depicts the results of the errors of the GPT3 and the GZTD-P models in different height intervals in the ZTD vertical interpolation at radiosonde stations.

As seen in Fig. 4, the GPT3 model exhibits obvious negative bias in each height interval in the layered ZTD vertical interpolation at radiosonde stations, with the maximum negative bias in the height interval from 4 to 8 km, which is close to − 2.5 cm. The ZTD of the layered vertical interpolation at the radiosonde stations calculated with the GPT3 model is smaller than the ZTD at the radiosonde stations. The GZTD-P model has a slight negative bias in the height interval from 0 to 4 km and a positive bias in the other height intervals. The ZTD of the layered vertical interpolation at the radiosonde stations calculated with the GZTD-P model is

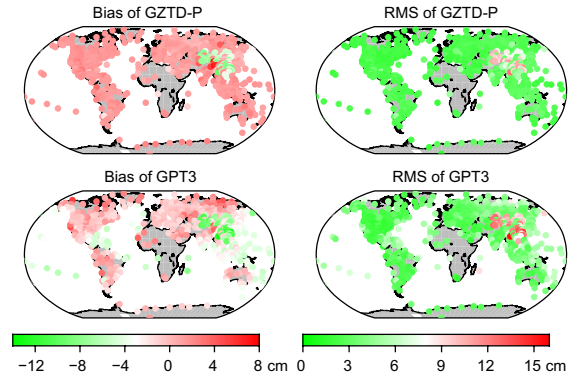

Fig. 3 The bias and RMS of GZTD-P model and GPT3 model validated at radiosonde stations

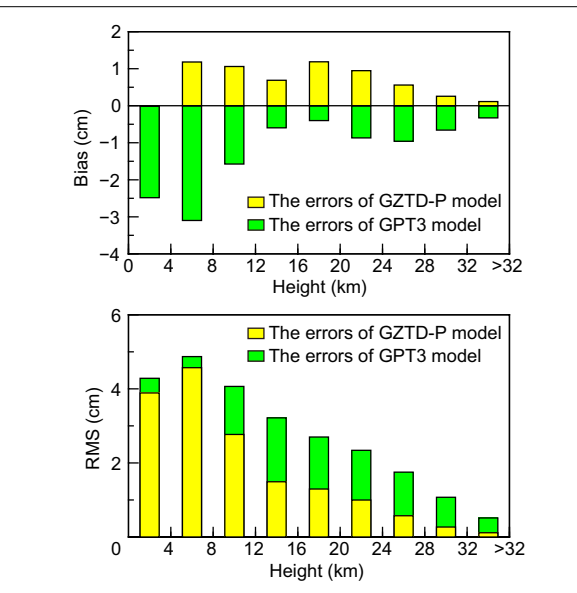

Fig. 4 The errors of the GZTD-P and GPT3 models in ZTD layered vertical interpolation in each height interval

larger than the ZTD at the radiosonde stations. Nonetheless, in most of the height intervals the GZTD-P model has a small absolute bias compared to the GPT3 model. Both the GPT3 and the GZTD-P models have the largest RMS values in the range from 4 to 8 km. This could be because ZWD (Zenith Wet Delay) is unstable at the elevations less than 10 km, and the value of ZWD gradually tends to 0 at the elevations greater than 10 km, allowing ZWD's effect to be ignored. ZTD is primarily affected by ZHD, which helps reduce RMS values in the elevations greater than 10 km. In the height above 4 km, both RMS values of the GPT3 model and the GZTD-P model gradually decreased with increasing elevation. Compared to the GPT3 model, the GZTD-P model shows little improvement in ZTD vertical interpolation accuracy in the 0–8 km range. In the elevations greater than 8 km, the GZTD-P model significantly outperforms the GPT3 model in ZTD vertical correction, indicating that the GZTD-P model performs better in ZTD vertical correction in high elevation region.

Model validation with MERRA-2 atmospheric reanalysis data

The ZTD vertical profile information of the MERRA-2 atmospheric reanalysis data in 2017 with a temporal resolution of six-hour is used to verify the accuracy of the GZTD-P and GPT3 models in the MERRA-2 atmospheric reanalysis data. The ZTD at the surface height is vertically interpolated to each layer of the MERRA-2. Finally, the performance of the ZTD obtained by the GZTD-P and the GPT3 models is shown in Table 3 and Fig. 5.

Table 3 shows that both the GZTD-P and the GPT3 models have a negative bias in the ZTD vertical interpolation of the MERRA-2 atmospheric reanalysis data, indicating that the ZTD calculated with the GZTD-P model and the GPT3 model is smaller than that with the MERRA-2 data. The bias of the GZTD-P model is 1.76 cm lower than that of the GPT3 model. The RMS of the GZTD-P model is 1.77 cm. The performance of the GZTD-P model is improved by 1.8 cm (50%) compared to the GPT3 model, indicating that the GZTD-P model has excellent correction effect and can better simulate the vertical characteristics of the tropospheric delays.

Figure 5 shows that the GPT3 model has a large negative bias over the globe, particularly in the equator and

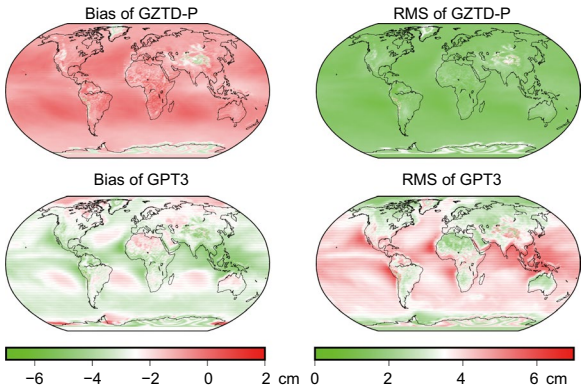

Fig. 5 The biases and RMSs of GZTD-P model and GPT3 model validated with MERRA-2 data

low latitude regions. Parts of Antarctica exhibit a positive bias. The GZTD-P model also has a negative bias across the globe, particularly in the Arctic Ocean, Central Asia, and Antarctica, indicating that the ZTD calculated with the GZTD-P model is smaller than the MERRA-2 integrated ZTD. In terms of RMS, the GPT3 model exhibits small RMS values in the northern and southern hemispheres, Africa, North America, South America, Europe, and Oceania, while large RMS values in the Pacific Ocean, Atlantic Ocean, and Indian Ocean. The possible reason is that the climate in these areas is complex and the water vapor is relatively rich, resulting in a more dramatic change in ZTD vertical direction. The GZTD-P model has better performance than the GPT3 model. The Arctic Ocean, Asia, and Antarctica exhibit large RMS errors, while the Pacific Ocean, Atlantic Ocean, Indian Ocean, and other regions have small RMS errors. Compared to the GPT3 model, the GZTD-P model performs better in low latitudes.

To examine the seasonal variation of the GPT3 model and the GZTD-P model in the ZTD layered interpolation accuracy of the MERRA-2 atmospheric reanalysis data, six grid points were chosen randomly, and the daily mean bias and RMS were calculated in 2017. Figures 6 and 7 show the time series at the six MERRA-2 grid points.

The GPT3 model has a clear negative bias in the selected grid points that are globally distributed, whereas the GZTD-P model has both positive and negative

Table 3 The performance of the GZTD-P and GPT3 models validated with MERRA-2 data

Models	Bias specifications (cm)			RMS specifications (cm)		
	Max	Min	Mean	Max	Min	Mean
GZTD-P	1.86	−5.29	−1.09	5.32	0.36	1.77
GPT3	0.67	−6.96	−2.85	6.97	1.10	3.57

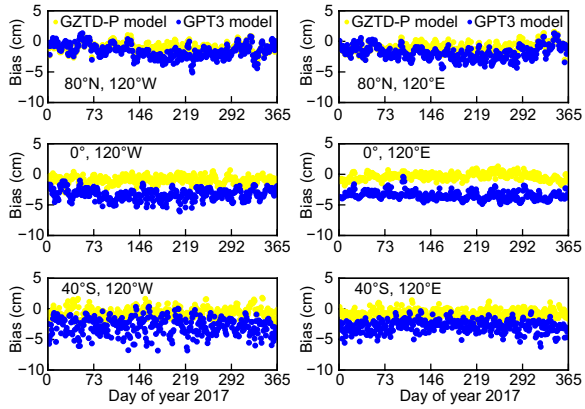

Fig. 6 Time series in the daily average bias at the six MERRA-2 grid points with the GZTD-P model and GPT3 model

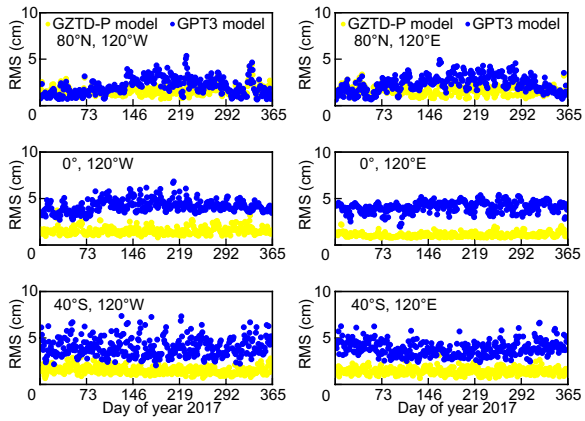

Fig. 7 Time series in the daily average RMS at the six MERRA-2 grid points with the GZTD-P model and GPT3 model

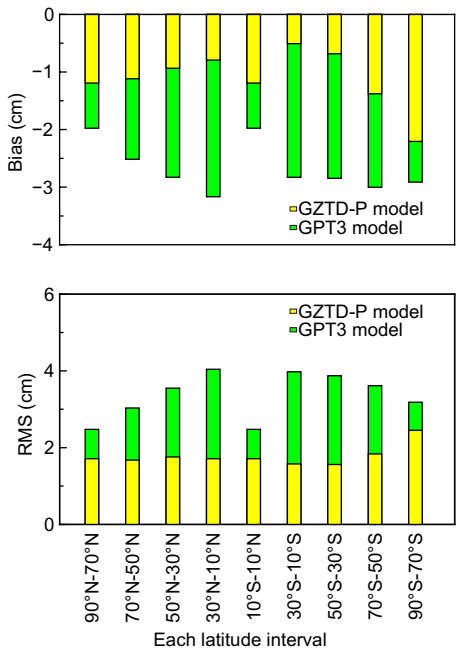

Fig. 8 The errors of the GZTD-P and GPT3 models in ZTD layered vertical interpolation in each latitude interval

biases. The GPT3 model shows the seasonal variation in RMS errors in the MERRA-2 ZTD vertical interpolation. Nonetheless, the GZTD-P model has better performance than the GPT3 model in terms of seasonal performance because the biases and RMS errors are small throughout the year.

Because ZTD varies with latitude, the globe is divided into nine latitude intervals of 20 degrees to further analyze the accuracy changes of the GPT3 model and GZTD-P model at different latitudes. Figure 8 summarizes the biases and RMSs of different latitude intervals calculated with the GPT3 model and the GZTD-P model in the MERRA-2 ZTD vertical interpolation.

Figure 8 shows that the GPT3 model has a clear negative bias value in each latitude interval in the MERRA-2 ZTD vertical interpolation. In the northern hemisphere, the bias gradually increases from high latitudes to low latitudes, reaching a maximum of −3 cm, whereas the bias of the GPT3 model in the southern hemisphere does not change significantly with latitude, displaying a large negative bias. The GZTD-P model also exhibits a clear negative bias in each latitude interval in the MERRA-2 ZTD vertical interpolation, indicating that the ZTD calculated with the GZTD-P and GPT3 models is smaller than the MERRA-2 ZTD value. In the northern hemisphere, the bias of the GZTD-P model decreases gradually as latitude decreases, which is the same in the southern hemisphere. It demonstrates that the GZTD-P model has the smallest bias in low latitude regions and the largest bias in high latitude regions. The largest negative bias in the latitude ranges from 70 to 90°S. In the northern hemisphere, the RMS of the GPT3 model increases gradually with decreasing latitude, which is the same in the southern hemisphere, indicating that the performance of the GPT3 model is worse in low latitudes, while it performs better in high latitudes. The RMS of the GZTD-P model changes little with latitude in the northern hemisphere, indicating that the latitude factor has little impact on the GZTD-P model's performance. The RMS of the GZTD-P model increases gradually with increasing latitude in the southern hemisphere with the largest RMS presented in the latitude range from 70 to 90°S, indicating that the GZTD-P model has higher accuracy in the lower latitudes of southern hemisphere and poor accuracy in high latitudes. In low-latitude regions around the world, the GZTD-P model has greater accuracy improvements

Table 4 The performance of the GZTD-P model and GPT3 model with different resolutions in the ZTD vertical interpolation of radiosonde data

Models	Number of parameters	Bias specifications (cm)			RMS specifications (cm)		
		Max	Min	Mean	Max	Min	Mean
GZTD-P-2	324 000	7.39	− 9.66	0.64	12.48	1.72	3.20
GPT3-1	1 296 000	5.27	− 13.35	− 1.78	15.76	1.53	4.16
GZTD-P-5	51 840	7.04	− 10.17	0.62	12.96	1.65	3.21
GPT3-5	51 840	5.11	− 13.42	− 1.89	15.53	1.46	4.21

than the GPT3 model, and there is some improvement in high-latitude regions. As a result, the GZTD-P model has superior ZTD vertical correction performance around the world.

Analysis of the accuracy of the GZTD-P model with different resolutions

When the GZTD-P model with a resolution of $2^\circ \times 2^\circ$ and the GPT3 model with a resolution of $1^\circ \times 1^\circ$ are compared, the performance of the GZTD-P model with a lower resolution is still better than that of the GPT3 model. One advantage of the sliding window algorithm is that users can change the size of the sliding window to obtain the model parameters at various resolutions as needed. The goal of developing a lower horizontal resolution version of the GZTD-P model is to enrich the model's applicability and speed up the tropospheric delay calculation process.

To test the accuracy of the GZTD-P model with different window sizes, a $5^\circ \times 5^\circ$ window size model parameter called GZTD-P-5 is created. The GZTD-P model with a resolution of $5^\circ \times 5^\circ$ is compared to a 5-degree version of the GPT3 model, known as the GPT3-5 model. Furthermore, the GZTD-P model's original resolution of $2^\circ \times 2^\circ$ is known as GZTD-P-2, and the GPT3 model's resolution of $1^\circ \times 1^\circ$ is known as GPT3-1. They are used in the accuracy comparison. The ZTD values of the layered profile integrated at 611 radiosonde stations were used to test the accuracy of the model vertical interpolation of ZTD at radiosonde stations. Table 4 and Figs. 9 and 10 show the models' performance in the vertical interpolation of radiosonde data.

Table 4 shows that the maximum RMS of the GZTD-P-5 model is 0.48 cm higher than the GZTD-P-2 model, while the minimum value is 0.07 cm lower. When the horizontal resolution of the GZTD-P-5 model is reduced, the accuracy of the GZTD-P-5 model is only 0.01 cm lower than that of the GZTD-P-2 model, which is nearly the same as the accuracy of the GZTD-P-2 model. The GPT3-5 model has a negative mean bias, whereas the GZTD-P-5 model has a positive mean bias, indicating that the ZTD calculated with the GPT3-5 model is

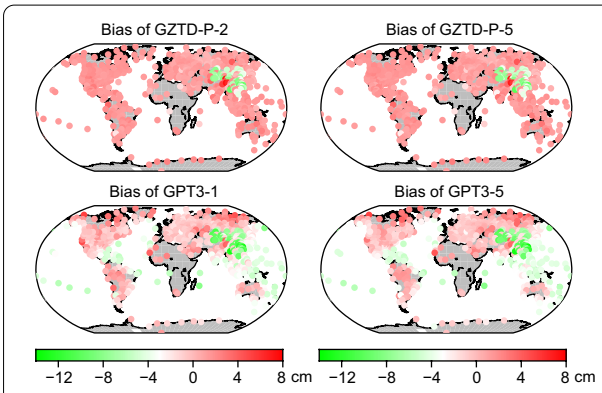

Fig. 9 Bias of the GZTD-P model and GPT3 model with different resolutions in the ZTD vertical interpolation of radiosonde over the globe

smaller than the radiosonde stations layer ZTD value, whereas the ZTD calculated with the GZTD-P model is larger. Compared to the GPT3-1 model, the absolute mean bias of the GZTD-P-5 model was reduced by 1.16 cm (65%), and the RMS error by 0.95 cm (23%). The absolute mean bias of the GZTD-P-5 model was reduced by 1.27 cm (67%) compared to the GPT3-5 model, and the RMS error by 1.00 cm (24%). As a result, with the same horizontal resolution, the accuracy of the GZTD-P-5 model is higher than that of the GPT3-5 model. Furthermore, the GZTD-P-5 model with the low horizontal resolution has higher accuracy than the GPT3-1 model with high horizontal resolution.

The GPT3-1 model has 1,296,000 model parameters for ZTD vertical adjustment, while the GZTD-P-2 model has 324,000 parameters, which is four times less than the former. The GZTD-P-5 model's performance is comparable to that of the GZTD-P-2 model. Meanwhile, the number of parameters in GZTD-P-5 is nearly six times less than that in GZTD-P-2, indicating that the GZTD-P-5 model optimizes the parameters while maintaining good performance. The number of model parameters in GZTD-P-5 is 51840, which is 25 times less than in GPT3-1 while providing better accuracy. Users should use the GZTD-P-5

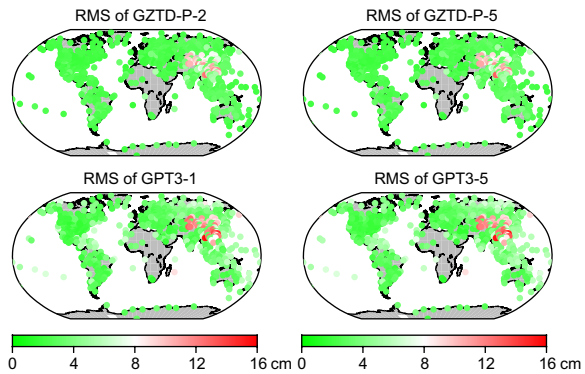

Fig. 10 RMS of the GZTD-P model and GPT3 model with different resolutions in the ZTD vertical interpolation of radiosonde over the globe

model for ZTD vertical correction to optimize model parameters and speed up the tropospheric delay calculation process.

Figures 9 and 10 show that the performance of the GZTD-P-5 model is nearly equal to that of the GZTD-P-2 model, with a small positive bias, indicating that the ZTD obtained with the GZTD-P-5 model is greater than the ZTD values at the radiosonde stations. The GZTD-P-5 model outperforms the GPT3 models in the Arctic Ocean, the junction of North and South America, West Africa, the Pacific, and Asia. As a result, the GZTD-P-5 model is recommended for users to select for ZTD vertical correction to further optimize the model parameters.

Conclusions

Zenith tropospheric delay correction relies heavily on the troposphere vertical stratification model. By investigating the characteristics of vertical tropospheric delay with respect to height, the GZTD-P model, an ERA5-based global model for vertical adjustment of zenith total delay using a piecewise function, is developed. MERRA-2 atmospheric reanalysis data and radiosonde station data are used to validate the GZTD-P model's accuracy. The GZTD-P model has excellent performance compared with the GPT3 model. The user only needs to provide the location and the Day of Year (DOY), and the ZTD value at the user's location can be calculated using the GZTD-P model for vertical correction. As a result, it is useful in global GNSS atmospheric sounding and GNSS precise positioning. Because only the ERA5 atmospheric reanalysis data are used for modeling in this paper, future work will consider combining multi-source data to construct a high-precision global tropospheric delay model.

Acknowledgements
The authors would like to thank ECMWF for providing the ERA5 grid data, NASA for providing the MERRA-2 grid data and IGRA for providing the radiosonde data in this study.

Author contributions
Conceptualization, LH and LL; methodology, GZ and LH; validation, YY, and JL; formal analysis, LZ; writing—original draft preparation, G.Z; writing—review and editing, LH, YY, JL, LZ, and LL; funding acquisition, LH, and LL.

Funding
This work was sponsored by the National Natural Science Foundation of China (41704027); Guangxi Natural Science Foundation of China (2020GXNSFBA297145; 2020GXNSFBA159033), and the "Ba Gui Scholars" program of the provincial government of Guangxi.

Data availability
Please contact author for data requests.

Declarations

Competing interests
The authors declare that they have no competing interests.

Author details
[1]College of Geomatics and Geoinformation, Guilin University of Technology, Guilin 541004, China. [2]College of Resources and Environment, Beibu Gulf University, Qinzhou 535011, China.

Received: 13 June 2022 Accepted: 14 November 2022
Published online: 28 November 2022

References

Black, H. D. (1978). An easily implemented algorithm for the tropospheric range correction. *Journal of Geophysical Research, 83*(B4), 1825–1828.
Böhm, J., Werl, B., Schuh, H. (2006). Troposphere mapping functions for GPS and very long baseline interferometry from European Centre for Medium-Range Weather Forecasts operational analysis data. *Journal of Geophysical Research: Solid Earth, 111*(B2).
Böhm, J., Heinkelmann, R., & Schuh, H. (2007). Short note: A global model of pressure and temperature for geodetic applications. *Journal of Geodesy, 81*, 679–683.
Böhm, J., Möller, G., Schindelegger, M., Pain, G., & Weber, R. (2015). Development of an improved blind model for slant delays in the troposphere (GPT2w). *GPS Solutions, 19*, 433.
Chen, P., Ma, Y., Liu, H., Zheng, N. (2020). A new global tropospheric delay model considering the spatiotemporal variation characteristics of ZTD with altitude coefficient. *Earth and Space Science. 7*, e2019EA000888.
Ding, J., & Chen, J. (2020). Assessment of Empirical Troposphere Model GPT3 Based on NGL's Global Troposphere Products. *Sensors., 20*(13), 3631.
Ding, M. (2020). Reducing ZHD-ZWD mutual absorption errors for blind ZTD model users. *Acta Geodaetica Et Geophysica., 55*(1), 51–62.
Gui, K., Che, H., Chen, Q., Zeng, Z., Liu, H., Wang, Y., Zheng, Y., Sun, T., Liao, T., Wang, H., & Zhang, X. (2017). Evaluation of radiosonde, MODIS-NIR-Clear, and AERONET precipitable water vapor using IGS ground-based GPS measurements over China. *Atmospheric Research., 197*, 461–473.
Hopfield, H. S. (1969). Two-Quartic tropospheric refractivity profile for correcting satellite data. *Journal of Geophysical Research, 74*(18), 4487–4499.
Huang, L., Chen, H., Liu, L., & Jiang, W. (2021a). A new high-precision global model for calculating zenith tropospheric delay. *Chinese Journal of Geophysics, 64*(3), 782–795.
Huang, L., Jiang, W., Liu, L., Chen, H., & Ye, S. (2019). A new global grid model for the determination of atmospheric weighted mean temperature in GPS precipitable water vapor. *Journal of Geodesy, 93*, 159–176.
Huang, L., Liu, L., & Yao, C. (2012). A zenith tropospheric delay correction model based on the regional CORS network. *Geodesy and Geodynamics, 3*(4), 53–62.

Huang, L., Mo, Z., Xie, S., Liu, L., Chen, J., Kang, C., & Wang, S. (2021b). Spatiotemporal characteristics of GNSS-derived precipitable water vapor during heavy rainfall events in Guilin. *China, Satellite Navigation, 2*, 13.
Huang, L. K., Zhu, G., Liu, L. L., Chen, H., & Jiang, W. P. (2021c). A global grid model for the correction of the vertical zenith total delay based on a sliding window algorithm. *GPS Solutions, 25*, 98.
Jin, S., & Su, K. (2020). PPP models and performances from single- to quad-frequency BDS observations. *Satellite Navigation, 1*, 16.
Krueger, E., Schüler, T., Hein, G. W., Martellucci, A., Blarzino, G. (2004). Galileo tropospheric correction approaches developed within GSTB-V1. In *Proceedings of ENC-GNSS 2004*, (pp. 16–19) May, Rotterdam.
Lagler, K., Schindelegger, M., Böhm, J., Krásná, H., & Nilsson, T. (2013). GPT2: empirical slant delay modelfor radio space geodetic techniques. *Geophysical Research Letters., 40*, 1069–1073.
Landskron, D., & Böhm, J. (2018). VMF3/GPT3: Refined discrete and empirical troposphere mapping functions. *Journal of Geodesy, 92*, 349–360.
Leandro, R., Santos, M., Langley, R. (2006). UNB neutral atmosphere models: development and performance. In *Proceedings of the ION NTM 2006 Monterey*, (pp. 564–573) January 18–20, California USA.
Leandro, R., Langley, R., & Santos, M. (2008). UNB3m_pack: A neutral atmosphere delay package for radiometric space techniques. *GPS Solutions, 12*, 65–70.
Li, H., Li, B., Lou, L., Yang, L., & Wang, J. (2017). Impact of GPS differential code bias in dual- and triple-frequency positioning and satellite clock estimation. *GPS Solutions, 21*(3), 897–903.
Li, H., Li, B., Xiao, G., Wang, J., & Xu, T. (2016). Improved method for estimating the inter-frequency satellite clock bias of triple-frequency GPS. *GPS Solutions, 20*(4), 751–760.
Li, W., & He, Y. (2021). Determination of tropospheric parameters from ERA surface data for space geodetic techniques. *Remote Sensing, 13*(19), 3813.
Li, W., Yuan, Y., Ou, J., Chai, Y., Li, Z., Liou, Y., & Wang, N. (2015). New versions of the BDS/GNSS zenith tropospheric delay model IGGtrop. *Journal of Geodesy, 89*(1), 73–80.
Li, W., Yuan, Y., Ou, J., & He, Y. (2018). IGGtrop_SH and IGGtrop_rH: two improved empirical tropospheric delay models based on vertical reduction functions. *IEEE Transactions on Geoscience and Remote Sensing, 6*(9), 5276–5288.
Li, W., Yuan, Y., Ou, J., Li, H., & Li, Z. (2012). A new global zenith tropospheric delay model IGGtrop for GNSS applications. *Chinese Science Bulletin, 57*(17), 2132–2139.
Li, X., Huang, J., Li, X., Lyu, H., Wang, B., Xiong, Y., & Xie, W. (2021). Multi-constellation GNSS PPP instantaneous ambiguity resolution with precise atmospheric corrections augmentation. *GPS Solutions, 25*, 107.
Ma, Y., Liu, H., Xu, G., & Lu, Z. (2021). Empirical orthogonal function analysis and modeling of global tropospheric delay spherical harmonic coefficients. *Remote Sensing., 13*, 4385.
Mohammed, J. (2022). Adaptive neuro fuzzy inference system for predicting sub-daily Zenith Wet Delay. *Geodesy and Geodynamics*. https://doi.org/10.1016/j.geog.2021.10.005
Molod, A., Takacs, L., Suarez, M., & Bacmeister, J. (2015). Development of the GEOS-5 atmospheric general circulation model: Evolution from MERRA to MERRA2. *Geosci. Model Dev., 8*, 1339–1356.
Nafisi, V., Urquhart, L., Santos, M. C., Nievinski, F. G., Bohm, J., Wijaya, D. D., Schuh, H., Ardalan, A. A., Hobiger, T., Ichikawa, R., & Zus, F. (2012). Comparison of ray-tracing packages for troposphere delays. *IEEE Transactions on Geoscience and Remote Sensing., 50*(2), 469–480.
Penna, N., Dodson, A., & Chen, W. (2001). Assessment of EGNOS tropospheric correction model. *Journal of Navigation, 54*, 37–55.
Randles, C. A., Da Silva, A. M., Buchard, V., Colarco, P. R., Darmenov, A., Govindaraju, R., Smirnov, A., Holben, B., Ferrare, R., Hair, J., & Shinozuka, Y. (2017). The MERRA-2 aerosol reanalysis, 1980 Onward. Part I: System description and data assimilation evaluation. *Journal of Climate., 30*, 6823–6850.
Saastamoinen, J. (1972). Contributions to the theory of atmospheric refraction. *Bulletin Géodésique, 105*(1), 279–298.
Schüler, T. (2014). The TropGrid2 standard tropospheric correction model. *GPS Solutions, 18*, 123–131.
Song, S., Zhu, W., Chen, Q. M., & Liou, Y. (2011). Establishment of a new tropospheric delay correction model over China area. *Science China (physics, Mechanics & Astronomy)., 54*(12), 2271–2283.
Sun, J., Wu, Z., & Yin, Z. (2017). A simplified GNSS tropospheric delay model based on the nonlinear hypothesis. *GPS Solutions, 21*(4), 1735–1745.
Sun, Z., Zhang, B., & Yao, Y. (2019). An ERA5-based model for estimating tropospheric delay and weighted mean temperature over China with improved spatiotemporal resolutions. *Earth and Space Science, 6*(10), 1926–1941.
Tang, Y., Liu, L., & Yao, C. (2013). Empirical model for mean temperature and assessment of precipitable water vapor derived from GPS. *Geodesy and Geodynamics, 4*(4), 51–56.
Thayer, G. D. (1974). An improved equation for the radio refractive index of air. *Radio Science, 9*(10), 803–807.
Xia, P., Xia, J., Ye, S., & Xu, C. (2020). A new method for estimating tropospheric zenith wet-component delay of GNSS signals from surface meteorology data. *Remote Sensing, 12*(21), 3497.
Xia, P., Ye, S., Guo, M., Jiang, W., & Xu, C. (2019). Retrieval of tropospheric refractivity profiles using slant tropospheric delays derived from a single ground-based global navigation satellite system station. *Earth and Space Science, 6*(7), 1081–1097.
Yang, F., Meng, X., Guo, J., Yuan, D., & Chen, M. (2021). Development and evaluation of the refined zenith tropospheric delay (ZTD) models. *Satellite Navigation, 2*, 21.
Yang, Y., Mao, Y., & Sun, B. (2020). Basic performance and future developments of BeiDou global navigation satellite system. *Satellite Navigation, 1*, 1.
Yao, Y., He, C., Zhang, B., & Xu, C. (2013). A new global zenith tropospheric delay model GZTD. *Chinese Journal of Geophysics, 56*(7), 2218–2227.
Yao, Y., Hu, Y., Yu, C., Zhang, B., & Guo, J. (2016). An improved global zenith tropospheric delay model GZTD2 considering diurnal variations. *Nonlinear Processes in Geophysics, 23*(3), 1–22.
Zhang, H., Yuan, Y., Wei, L., Zhang, B., & Ou, J. (2018). A grid-based tropospheric product for China using a GNSS network. *Journal of Geodesy, 92*(7), 765–777.
Zhang, W., Lou, Y., Liu, W., Huang, J., & Zhang, H. (2020). Rapid troposphere tomography using adaptive simultaneous iterative reconstruction technique. *Journal of Geodesy, 94*, 76.
Zhao, J., Song, S., Chen, Q., Zhou, W., & Zhu, W. (2014). Establishment of a new global model for zenith tropospheric delay based on functional expression for its vertical profile. *Chinese Journal of Geophysics, 57*(10), 3140–3153.
Zhou, F., Cao, X., Ge, Y., & Li, W. (2020). Assessment of the positioning performance and tropospheric delay retrieval with precise point positioning using products from different analysis centers. *GPS Solutions, 24*, 12.
Zhou, Y., Lou, Y., Zhang, W., Bai, J., & Zhang, Z. (2021). An improved tropospheric mapping function modeling method for space geodetic techniques. *Journal of Geodesy, 95*, 98.
Zhu, G., Huang, L., Liu, L., Li, C., Li, J., Huang, L., Zhou, L., & He, H. (2021). A new approach for the development of grid models calculating tropospheric key parameters over China. *Remote Sensing., 13*(17), 3546.
Zus, F., Dick, G., Douša, J., Heise, S., & Wickert, J. (2014). The rapid and precise computation of GPS slant total delays and mapping factors utilizing a numerical weather model. *Radio Science, 49*(3), 207–216.

Publisher's Note